Supporting Information:

Engineering Interconnected Open-Porous Particles via Microfluidics using Bijel Droplets as Structural Templates

Mina Masaoka[a], Hiroaki Ishida[a], Takaichi Watanabe[a]*, and Tsutomu Ono[a]

[a] Department of Applied Chemistry, Graduate School of Natural Science and Technology, Okayama University, 3-1-1, Tsushima-naka, Kita-ku, Okayama, 700-8530, Japan

*Email: wata-t@okayama-u.ac.jp, Phone: +81-86-251-8072

Table S1. Amount added for ternary phase diagram drawing (mass) in the absence of silica particles and CTAB.

Sample name	ETPTA [g]	Ethanol [g]	Water [g]
A-1	0.101	0.900	1.423
A-2	0.300	0.705	0.838
A-3	0.400	0.600	0.628
A-4	0.500	0.501	0.453
A-5	0.601	0.401	0.329
A-6	0.701	0.299	0.213
A-7	0.801	0.201	0.131
A-8	0.900	0.103	0.048

Table S2. Amount added for ternary phase diagram drawing (volume) in the absence of silica particles and CTAB.

Sample name	ETPTA [mL]	Ethanol [mL]	Water [mL]
A-1	0.091	1.138	1.423
A-2	0.271	0.893	0.838
A-3	0.361	0.760	0.628
A-4	0.450	0.634	0.453
A-5	0.542	0.507	0.329
A-6	0.632	0.379	0.213
A-7	0.722	0.254	0.131
A-8	0.810	0.130	0.048

Table S3. Amount added for ternary phase diagram drawing (volume fractions) in the absence of silica particles and CTAB.

Sample name	ETPTA [-]	Ethanol [-]	Water [-]
A-1	0.034	0.429	0.537
A-2	0.135	0.446	0.419
A-3	0.206	0.435	0.359
A-4	0.293	0.413	0.295
A-5	0.393	0.368	0.239
A-6	0.516	0.310	0.174
A-7	0.652	0.230	0.118
A-8	0.820	0.131	0.048

Table S4. Amount added for ternary phase diagram drawing (mass) with silica particles and CTAB

Sample name	ETPTA [g]	Ethanol [g]	100 mM CTAB / Ethanol [g]	Water [g]	Silica nanoparticles [g]
E10	0.100	0.823	0.086	1.518	0.782
E20	0.200	0.722	0.089	1.287	0.663
E30	0.300	0.624	0.086	0.952	0.491
E40	0.401	0.525	0.087	0.735	0.378
E50	0.500	0.423	0.088	0.397	0.205
E60	0.601	0.323	0.086	0.212	0.109
E70	0.700	0.221	0.085	0.143	0.074
E80	0.800	0.121	0.085	0.102	0.052
E90	0.901	0.024	0.082	0.021	0.011

Table S5. Amount added for ternary phase diagram drawing (volume) with silica particles and CTAB

Sample name	ETPTA [mL]	Ethanol [mL]	Water [mL]
E10	0.090	1.146	1.518
E20	0.180	1.021	1.287
E30	0.270	0.893	0.952
E40	0.361	0.769	0.735
E50	0.450	0.642	0.397
E60	0.541	0.512	0.212
E70	0.631	0.382	0.143
E80	0.720	0.256	0.102
E90	0.812	0.130	0.021

Table S6. Amount added for ternary phase diagram drawing (volume fractions) with silica particles and CTAB.

Sample name	ETPTA [-]	Ethanol [-]	Water [-]
E10	0.033	0.416	0.551
E20	0.073	0.410	0.517
E30	0.128	0.422	0.450
E40	0.194	0.413	0.394
E50	0.302	0.431	0.267
E60	0.428	0.405	0.167
E70	0.545	0.331	0.124
E80	0.668	0.238	0.094
E90	0.843	0.135	0.022

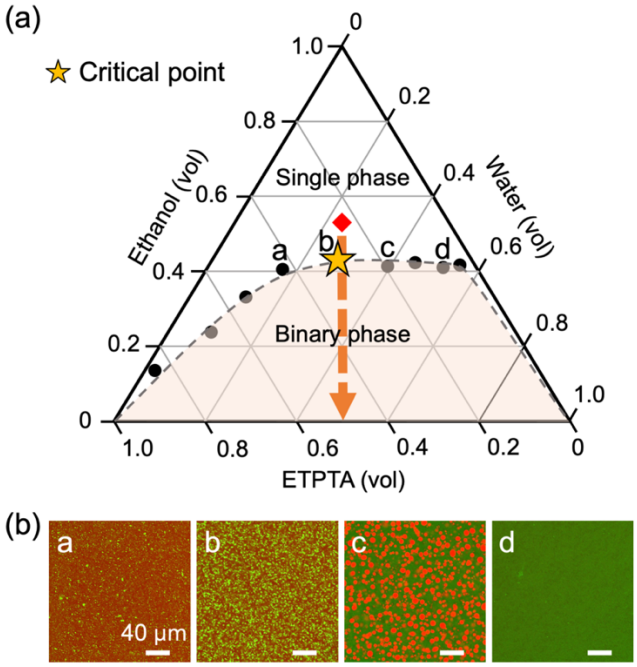

Figure S1. (a) Ternary phase diagram of the ETPTA/ethanol/water (dispersed phase) system. The star symbol and dashed line indicate the critical point and binodal line, respectively. The diamond symbol indicates the standard initial dispersed phase composition determined from the phase mapping. **(b)** CLSM images of the phase-separated structure of the dispersed phase solutions at different conditions (red: oil phase and green: fluorescent silica particles). The average droplet diameters in condition **a** and **c** were 1.6 μm and 5.9 μm, respectively.

Table S7. Amount of each substance added into the dispersed phase conditions [mL].

Entry	ETPTA	Ethanol	200 mM CTAB / ethanol	Water	Ludox TMA	Sicastar	Darocur 1173
1	2.12	4.77	-	0.77	1.01	0.52	0.11
2	2.12	4.66	0.11	0.77	1.01	0.52	0.11
3	2.12	4.32	0.45	0.77	1.01	0.52	0.11
4	2.12	3.87	0.90	0.77	1.01	0.52	0.11
5	2.12	3.42	1.35	0.77	1.01	0.52	0.11
6	2.12	2.52	2.25	0.77	1.01	0.52	0.11
7	2.12	4.77	-	2.12	-	-	0.11
8	2.12	4.32	0.45	2.12	-	-	0.11

Bare silica particles : Florescent silica particles = 97 : 3 (w/w)

Table S8. Summary of pH values of the dispersed phase.

Sample	Silica particle [wt%]	CTAB [mM]	pH
Ludox TMA	34	0	3.6
Entry1	5	0	4.7
Entry2	5	2.5	4.8
Entry3	5	10	4.7
Entry4	5	20	4.6
Entry5	5	30	4.6
Entry6	5	50	4.7
Entry7	0	0	4.7
Entry8	0	10	4.7

Calculation of coverage of CTAB onto silica particles (θ_{CTAB})

The coverage of CTAB on silica particles (θ_{CTAB}) was calculated from the following equations.

$d_{silica} = 22\ [nm]$

$(N_{silanol}) = 4.0\ [/nm^2]$ [1]

$N_{CTAB} = \left(V_{dispersed}\ [m^3]\right) \times \left(C_{CTAB}\ [{}^{mol}/_{m^3}\right) \times (N_A\ [{}^{1}/_{mol}])$

$(N_{silicaNPs}) = \left(V_{silicaNPs\_dispersed}[m^3]\right) /[\frac{4}{3}\pi({}^{d_{silica}}/_{2})^3[m^3]]$

$\left(N_{silanol\_on\_particle}\right) = d_{silica} \times 2\pi \times 4.0 \times N_{silicaNPs}$

$\theta_{CTAB} = N_{CTAB}/N_{silanol\_on\_particle}$

where d_{silica}: diameter of silica particles [nm], $N_{silanol}$: the number of silanol groups per unit area $[/nm^2]$, N_{CTAB}: the number of CTAB in the dispersed phase, $V_{dispersed}$: the volume of dispersed phase $[m^3]$, N_A: Avogadro constant [/mol], $N_{silicaNPs}$: the number of silica particles in the dispersed phase, $N_{silanol\_on\_particle}$: the total number of silanol groups on the particles in the dispersed phase, $N_{silanol\_on\_particle}$: the total number of silanol groups on the particles in the dispersed phase, and θ_{CTAB}: the surface coverage of CTAB on the silica particles [%].

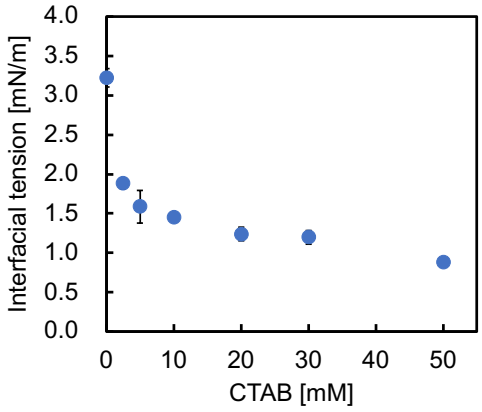

Figure S2 Interfacial tension between ETPTA and water as a function of CTAB concentrations.

Table S9. Compositions of the systems for measuring interfacial tensions between water and CTAB-modified silica particles.

Silica particle [wt%]	CTAB [mM]	CTAB [g]	Water [mL]	Ludox TMA [mL]
5	0	0	1.414	1.153
5	2.5	0.009	1.414	1.153
5	5	0.018	1.414	1.153
5	10	0.036	1.414	1.153
5	20	0.072	1.414	1.153
5	30	0.108	1.414	1.153
5	50	0.180	1.414	1.153

Table S10. Interfacial tensions (γ) and viscosity of the continuous phase (μ_c) for each preparation.

	Silica particles [wt%]	CTAB [mM]	γ [mN/m]	μ_c [mPa s]
Entry1	5	0	3.2	4.2
Entry2	5	2.5	1.9	4.4
Entry3	5	10	1.5	4.4
Entry4	5	20	1.2	4.4
Entry5	5	30	1.2	4.3
Entry6	5	50	0.9	4.4
Entry7	0	0	3.9	3.9
Entry8	0	10	1.9	4.0

Table S11. Characteristics of CTAB-modified silica particles dispersed in water measured at pH 3.0.

Sample	Silica particle [wt%]	CTAB [mM]	Zeta potential [mV]	Coverage θ_{CTAB} [%]	Relative surface coverage [%]*
Entry1	5	0	-28.5	0	0
Entry2	5	2.5	-27.4	6.3	3.9
Entry3	5	10	-23.3	25.0	18.2
Entry4	5	20	-17.2	49.7	39.6
Entry5	5	30	-7.8	74.3	72.7
Entry6	5	50	0.4	122.8	100

$$*Relative\ surface\ coverage\ [\%] = \{1 - \frac{[absolute\ zeta\ potential\ of\ CTAB{-}modified\ silica\ particles]}{[zeta\ potential\ of\ bare\ silica\ particles\ (= 28.5\ mV)]}\} \times 100$$

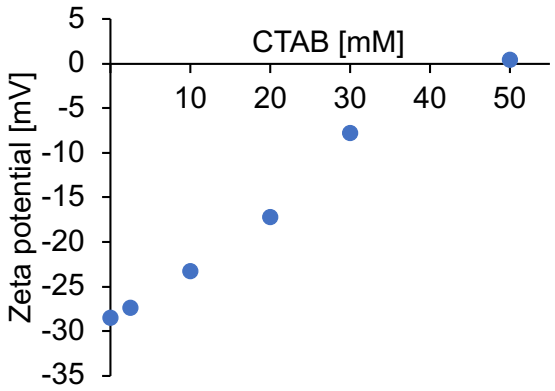

Figure S3. Variation of zeta potential for silica particles with CTAB concentrations.

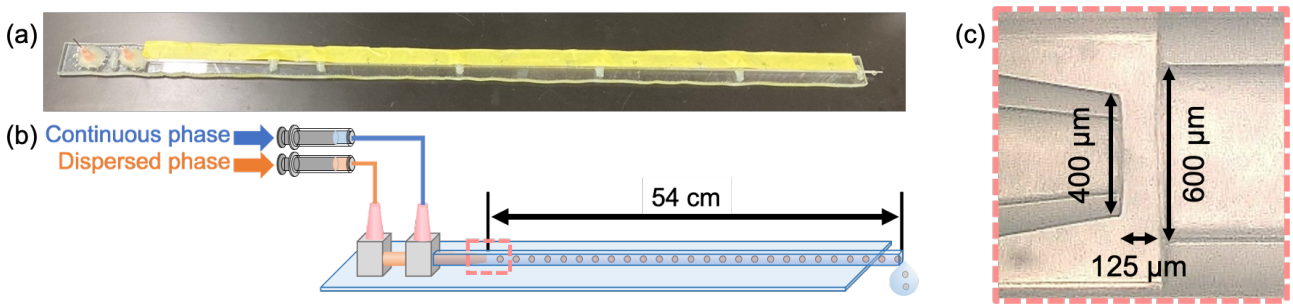

Figure S4. (a) Photograph of the device, **(b)** schematic of the device, and **(c)** emulsification point of in the device.

Flow conditions to generate monodisperse droplets

Droplet formation in microfluidics is known to be influenced by a variety of factors, including the flow rates of the phases, their viscosities, interfacial tensions, and the geometry of the channel [2]. In microfluidics, droplet formation generally occurs through two mechanisms: dripping and jetting. These behaviors are typically characterized by the Capillary number (Ca_c) of the continuous phase, defined as $Ca_c = \mu_c v_c/\gamma$, where μ_c, v_c, and γ are the viscosity, velocity of the continuous phase, and interfacial tension, and by the Weber number (We_d) of the dispersed phase, expressed as $We_d = \rho_d d_{tip} {v_d}^2/\gamma$, where ρ_d, d_{tip}, and v_d are the density of the dispersed phase, inner diameter of capillary tube, and velocity of the dispersed phase. To determine flow conditions that generate monodisperse emulsion droplets, we constructed a state diagram showcasing the approximate boundary between dripping and jetting within our microfluidic setup, represented by $Ca_c$and We_d. Our findings indicated that monodisperse droplets were generated within the dripping regime shown as closed circle symbols in **Figure S5**. Conversely, in the jetting regime shown as closed diamond symbols, droplet formation became unstable, leading to polydisperse droplets.

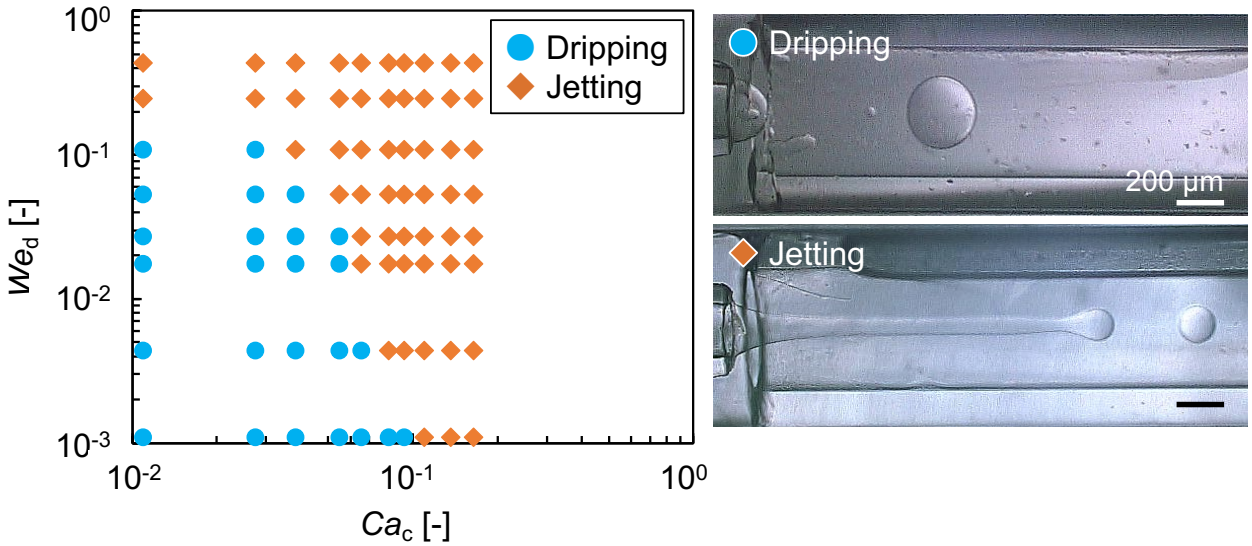

Figure S5. Formation of monodisperse droplets using a microfluidic device. State diagram of the dripping to jetting transition on the Capillary number of the outer flow and the Weber number of the inner flow of a capillary microfluidic device. Blue circle symbols represent dripping, while orange diamond symbols represent jetting.

Table S12. Flow conditions of each sample preparation.

Sample	Flow pattern	Capillary number (Ca_c)	Weber number (We_d)	Viscosity ratio (μ_d/μ_c)	Flow rate ratio (Q_d/Q_c)
Entry1	Dripping	0.012	0.00049	4.2	2×10^{-2}
Entry2	Dripping	0.021	0.00084	4.3	2×10^{-2}
Entry3	Dripping	0.027	0.00109	4.4	2×10^{-2}
Entry4	Dripping	0.032	0.00128	4.3	2×10^{-2}
Entry5	Dripping	0.033	0.00132	4.3	2×10^{-2}
Entry6	Dripping	0.045	0.00182	4.3	2×10^{-2}
Entry7	Dripping	0.010	0.00039	3.9	2×10^{-2}
Entry8	Dripping	0.021	0.00080	4.0	2×10^{-2}

Change in the droplet diameter as a function of distance after droplet formation

The volume change of the droplets after their formation was calculated from the optical microscopy images in the microchannel as shown in **Figure S6**. The volume of a droplet (V) after droplet formation was normalized by the initial droplet volume (V_0). As shown in **Figure S6**, the volume of droplets decreased until the droplets reached at 20 cm downstream, then the value was approximately constant at 0.8 (20% volume reduction). However, considering the initial droplet composition contained 53 vol% ethanol, it can be estimated that around 33 vol% ethanol remains when the volume reduction stopped. This discrepancy likely arises from the assumption that only ethanol diffuses from the droplet to the continuous phase, whereas actually, there is a mutual diffusion of ethanol and water, and an influx of cyclohexane into the droplets.

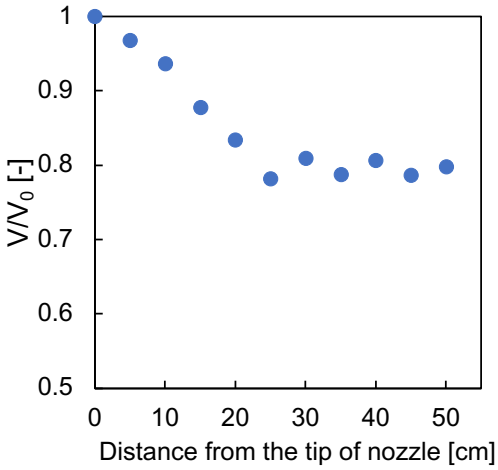

Figure S6. Droplet volume variation with distance from the nozzle tip, where V_0 is the initial volume and V is the volume at a specified distance from the tip.

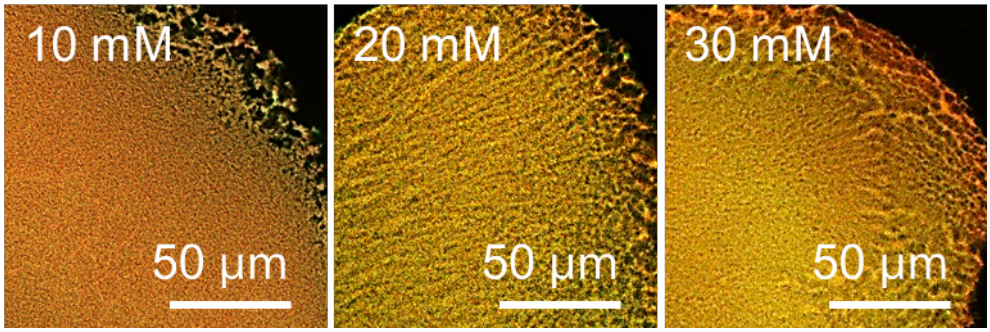

Figure S7. Magnified CLSM images of the particles prepared with different CTAB concentrations. These phase-separated structures were classified as "bicontinuous" as shown in Figure 2.

Measurement of average pore size by ImageJ

The measurement of the average pore size of particles was performed through SEM image analysis. The subsequent workflow outlines the procedural steps taken to quantify the pore area based on the SEM images. This quantification is achieved by processing the SEM images via the ImageJ software (version 1.53). The detailed processing steps were illustrated in **Figure S8**.

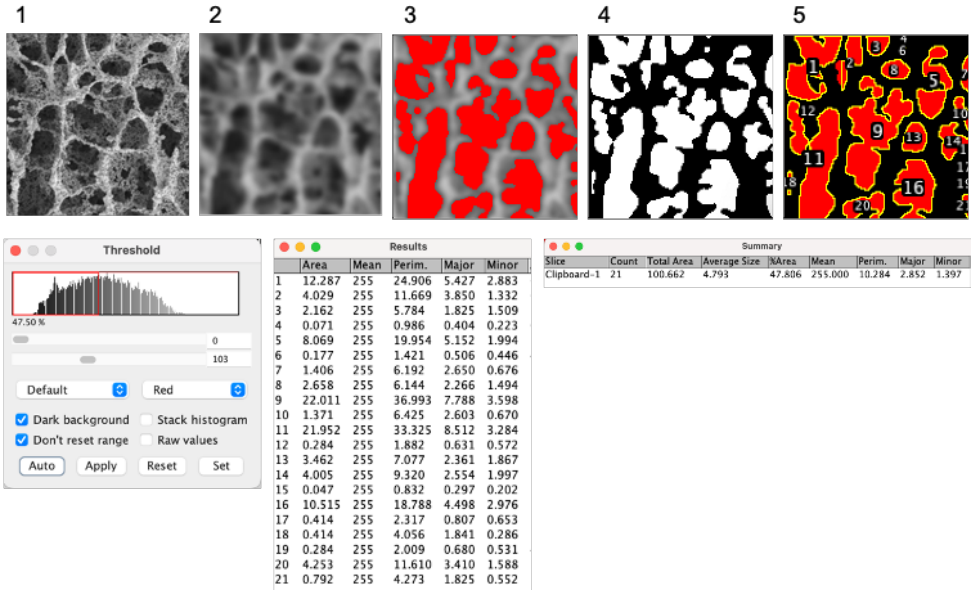

	Area	Mean	Perim.	Major	Minor
1	12.287	255	24.906	5.427	2.883
2	4.029	255	11.669	3.850	1.332
3	2.162	255	5.784	1.825	1.509
4	0.071	255	0.986	0.404	0.223
5	8.069	255	19.954	5.152	1.994
6	0.177	255	1.421	0.506	0.446
7	1.406	255	6.192	2.650	0.676
8	2.658	255	6.144	2.266	1.494
9	22.011	255	36.993	7.788	3.598
10	1.371	255	6.425	2.603	0.670
11	21.952	255	33.325	8.512	3.284
12	0.284	255	1.882	0.631	0.572
13	3.462	255	7.077	2.361	1.867
14	4.005	255	9.320	2.554	1.997
15	0.047	255	0.832	0.297	0.202
16	10.515	255	18.788	4.498	2.976
17	0.414	255	2.317	0.807	0.653
18	0.414	255	4.056	1.841	0.286
19	0.284	255	2.009	0.680	0.531
20	4.253	255	11.610	3.410	1.588
21	0.792	255	4.273	1.825	0.552

Slice	Count	Total Area	Average Size	%Area	Mean	Perim.	Major	Minor
Clipboard-1	21	100.662	4.793	47.806	255.000	10.284	2.852	1.397

Figure S8. Workflow for measuring average pore size of the particles: (1) Selection of representative SEM images depicting the product surface; (2) Application of Gaussian Blur to adjust image sharpness; (3) Binarization of the image using adaptive thresholding to distinguish pores from the polymer matrix; (4) Utilization of thresholding techniques to enhance visualization of the interfaces; (5) Quantitative analysis to determine the average pore area using the particle analysis feature.

Phase-separated structure from each dispersed phase composition

To confirm the separation pattern as the phase separation progressed in each dispersed phase composition, solutions with compositions of ETPTA : ethanol : water = 0.45 : 0.10 : 0.45 (v/v) were observed under each condition, assuming that only ethanol diffused. The silica particles were added at the starting point prior to ethanol diffusion with a silica particle concentration of 8 wt% and a CTAB concentration of 20 mM (**Table S13**) and observed with CLSM.

Table S13. Amount of each substance added to prepare phase-separated structure [mL].

	ETPTA	Ethanol	200 mM CTAB / ethanol	Water	Ludox TMA	Sicastar
Entry1	0.94	0.20	-	0.34	0.45	0.23
Entry3	0.94	-	0.20	0.34	0.45	0.23
Entry7	0.94	0.20	-	0.94	-	-
Entry8	0.94	-	0.20	0.94	-	-

As shown in **Figure S9**, entry 3_bulk, which contained both silica particles and CTAB, demonstrated the adsorption of silica particles at the interface between the oil and water phases, and the oil and water phases maintained bicontinuous structures. Conversely, in entry 7, which lacked both additives, coalescence occurred. Entry 1, containing excess amount of silica particles exhibited an O/W type phase separation. Meanwhile, entry 8, with only CTAB also showed coalescence.

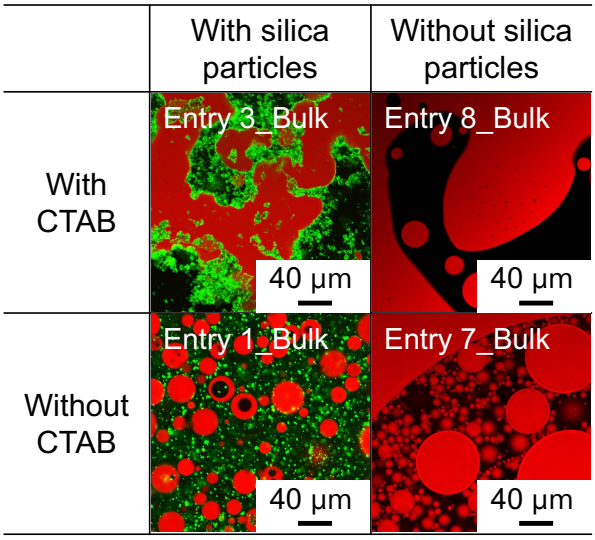

Figure S9. CLSM images of dispersed phase (bulk) solutions containing silica particles at the UV irradiated locations under conditions with and without silica and/or CTAB (red : oil phase, green : fluorescent silica particles).

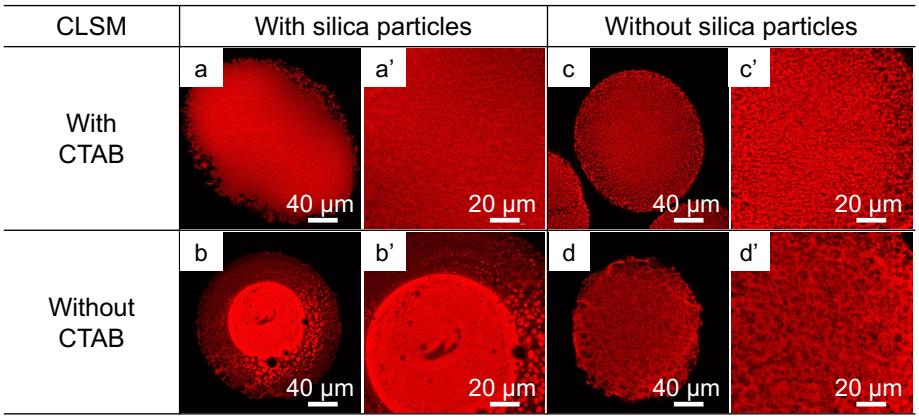

Figure S10. CLSM images of the open-porous particles prepared under different conditions of the dispersed phase: **(a)** entry 3, **(b)** entry 1, **(c)** entry 8 and **(d)** entry 7. Magnified surface images of **(a')** entry 3, **(b')** entry 1, **(c')** entry 8, and **(d')** entry 7. The oil phase is shown in red color.

Change in the porous structure as increasing time after the onset of phase separation

To observe the change in the porous structure as increasing time after phase separation, droplets during phase separation were polymerized by UV irradiation at different locations from an emulsification point.

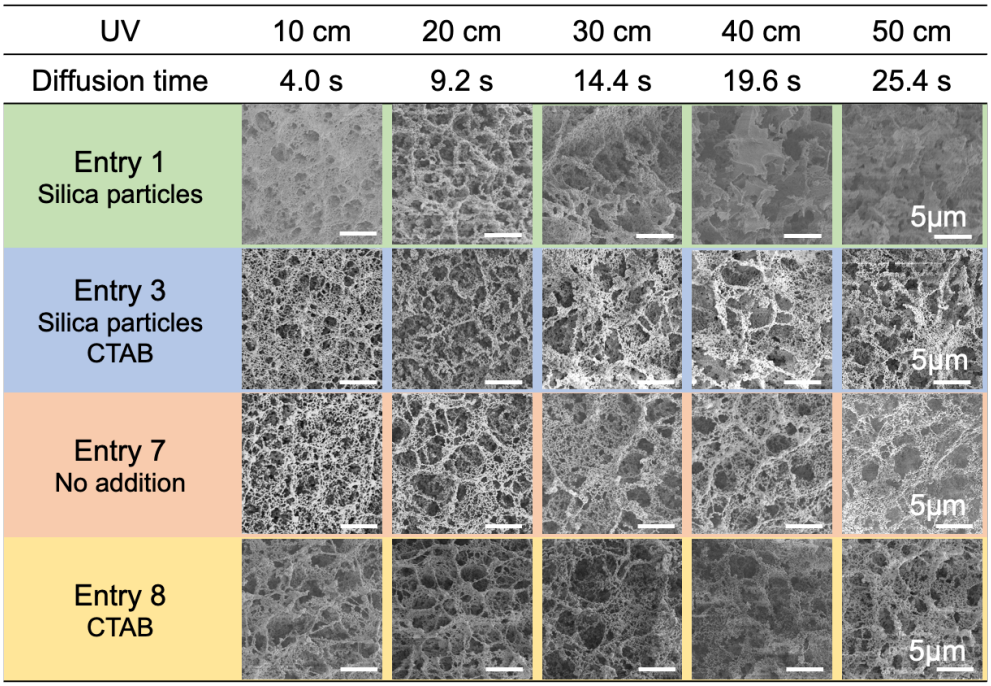

Figure S11. SEM images of the particle surface at the UV irradiated locations under conditions with and without silica particles and/or CTAB.

References

(1) Boakye-Ansah, S.; Khan, M. A.; Haase, M. F. Controlling Surfactant Adsorption on Highly Charged Nanoparticles to Stabilize Bijels. *J. Phys. Chem. C* **2020**, *124* (23), 12417–12423.

(2) Choi, S.-W.; Cheong, I. W.; Kim, J.-H.; Xia, Y. Preparation of Uniform Microspheres Using a Simple Fluidic Device and Their Crystallization into Close-Packed Lattices. *Small* **2009**, *5*, 454−459.